Available online at https://link.springer.com/journal/42241
http://www.jhydrodynamics.com
Journal of Hydrodynamics, 2019
https://doi.org/10.1007/s42241-019-0054-9

Effects of finite water depth and lateral confinement on ships wakes and resistance.

Clément Caplier[1], Germain Rousseaux[1], Damien Calluaud[1], Laurent David[1]

1. *Institut Pprime – CNRS, University of Poitiers, ISAE-ENSMA, 86962 Futuroscope Chasseneuil, France*
(Received October 18, 2018, Revised December 20, 2018, Accepted January 10, 2019, Published online June 6, 2019)

Abstract: Wash waves produced by ships disintegrate river banks and coastal lines. This phenomenon of bank erosion is mainly due to the height of the waves. Various factors govern the formation of these waves and their amplitudes: the geometry of the water channel, the shape and the speed of the boat, etc. These factors play an important role on the wave generation but also on the resistance of the ship and so on its fuel consumption. Whether to study the impact of wash waves on the ship's environment or its resistance, the analysis of the generated wake is essential. Hence a fine characterization of the wave field is necessary. This study proposes a comparison of wakes generated by two generic ships based on a Wigley hull with block coefficients 0.67 and 0.89 respectively representative of maritime and fluvial ships. The wakes generated in deep water and confined water configurations have been measured for different Froude numbers with a non-intrusive optical stereo-correlation method, giving access to a detailed and complete definition of the generated wave fields. The resistance of the ship hulls has been measured in deep and confined water configurations with a hydrodynamic balance. The results permit to study the influence of both hull and water channel geometries on the ship wake, on the amplitude of the far-field generated waves and on the near-field hydrodynamic response. Moreover, resistance curves are obtained for both configurations and highlight the effect of both hull and water channel geometries on the resistance coefficient of the ship. A comparison of the resistance curves with or without the ship trim is conducted and shows the influence of the trim on the resistance coefficient in the different ship speed regimes.

Key words: Ship wakes, wash waves, confined water, ship resistance

Introduction

Various factors govern the generation and the amplitude of wash waves: the bathymetry of the water channel, the geometry and the speed of the ship, the hull shape.

On the one hand, when a ship navigates in a waterway of finite water depth, the effects of confinement result in a change of the shape of the generated wave field[1-7]. As the shallow water wake shape highly depends on both the water depth and the ship speed, the non-dimensional height-based Froude number $F_h = \mathrm{U}/\sqrt{\mathrm{gh}}$ (where $U(m.s^{-1})$ is the ship speed, $g(m.s^{-2})$ the gravity and $h(m)$ the water depth in the waterway), allows to distinguish various regimes[3,8]. For $F_h < 0.60$, there are no visible effects of finite water depth and the wave field is similar to the deep water V-shaped Kelvin wake[9]. This wake is composed of transverse and divergent waves, respectively perpendicular and oblique with respect to the advancing line of the ship. These two wave systems superimpose on a cusp line which defines the envelop of the wake and forms the typical Kelvin angle $\alpha = 19.47°$ with respect to the advancing line. That angle remains constant until a threshold ship speed from which it decreases[10-17]. For $0.60 < F_h < 1.00$ the wake is transcritical from an undulatory point of view, its angle increases with the ship speed, as well as the wavelength of the transverse waves. At the particular speed corresponding to $F_h = 1.00$, *i.e.* $\mathrm{U} = \sqrt{\mathrm{gh}}$, the wake is critical and the envelop of the wake consists in a perpendicular bow wave in front of the ship ($\alpha = 90°$). In addition, the transverse waves disappear and the wake is only composed of divergent waves. For $F_h > 1.00$ the wake is supercritical and the bow waves folds backwards to the ship with respect to the Froude number as $\alpha = \mathrm{asin}(1/F_h)$. This behavior is reminiscent of the Mach cone in supersonic aerodynamics. On the other hand, important hydrodynamic effects appear around the ship, when the waterway is confined both vertically and laterally. It has been highlighted by Scott Russell[18], through his observations and experiments in narrow and shallow waterways during the nineteenth century. The Scottish engineer has pointed out the decreasing of the water level around the ship, whose impact on the river banks is important. Moreover, the ship is subject to squat and there is a risk of touching the ground. Nevertheless, the major effect highlighted by Scott Russell is the apparition of a bow wave in front

[1] **Biography:** Clément Caplier (1990-), Male, PhD,
Corresponding author: Clément Caplier,
E-mail: clement.caplier@univ-poitiers.fr

of the ship, causing an increase of the ship resistance. The effects of both vertical and lateral confinement on the ship resistance are different[18-20]. Indeed, for a given water depth, the effect of the lateral confinement consists in the apparition of a peak in the resistance for a ship speed U=$\sqrt{gh}$, corresponding to a height-based Froude number $F_h = 1.00$. The smaller is the width of the water channel, the higher is the peak of resistance at $F_h = 1.00$. For a given channel width, the decrease of the water depth results also in the apparition of a peak in the resistance curve, but for a different height-based Froude number. Moreover, the smaller is the water depth, the lower is the speed that corresponds to the peak of resistance. In the case of both lateral and vertical confinement, hydraulic effects appear and the resulting resistance curve highlights two critical height-based Froude numbers. The hydrodynamics theory established by Schijf[21] leads to the theoretical expressions given in (1) and (2) (they are based on the mass conservation and Bernoulli equations):

$$F_{h1} = \left[2\sin\left(\frac{\text{asin}(1-m)}{3}\right)\right]^{3/2} \quad (1)$$

$$F_{h2} = \left[2\sin\left(\frac{\pi-\text{asin}(1-m)}{3}\right)\right]^{3/2} \quad (2)$$

where the critical Froude numbers are given as a function of the blockage ratio of the waterway $m = A_s/A_c$ (where A_s is the immersed cross-section of the ship and A_c the cross-section of the canal), which reflects the importance of both vertical and lateral confinement. These two height-based critical Froude numbers F_{h1} and F_{h2} are plotted against the blockage ratio m in Figure 1. An increase of the blockage ratio, *i.e.* a decrease of the water depth and/or a narrowing of the width of the waterway, leads to a widening of the hydraulic transcritical region where the confined water effects occur.

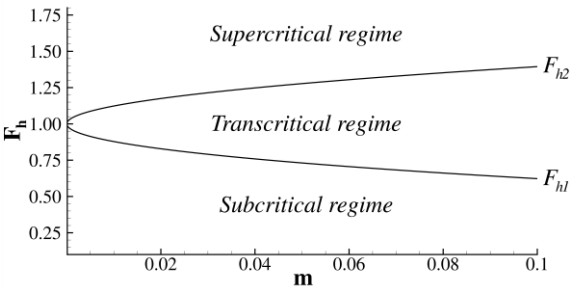

Fig. 1: Schijf's diagram. The curve represents the theoretical values of the critical height-based Froude numbers F_{h1} and F_{h2} given by Schijf's theory[21] as a function of the blockage ratio $m = A_s/A_c$.

Recent studies on the effects of the confinement of the waterway on ship wakes and the link with the ship resistance are built on numerical investigations[22-24]. These numerical models are based on the resolution of Reynolds-Averaged Navier-Stokes (RANS) equations, closed with k-ω SST or k-ε turbulence models. The free-surface capturing strategy is based on a multi-phase approach using Volume Of Fluid (VOF) method, and the ship motions are simulated with a dynamic mesh technique. However, the confinement has a strong impact on the energy repartition in the ship wake and on both hydraulic and undulatory components of the wake[25]. These effects are still not completely described numerically or theoretically, and experimental studies on small-scale models are thus necessary to feed the analysis.

1. Experimental setup

1.1 *Maritime and river ship hulls*

The two ship hulls are based on a Wigley[26] hull with a rectangular section. This hull form is mathematically defined by the parabolic expression given in (3):

$$y=f(x) = \frac{B}{2}\left[1 - \left(\frac{2x}{L}\right)^{n=2}\right] \quad (3)$$

in which x and y represent respectively the longitudinal and transversal axes of the ship. L represents the length of the hull ($L = 1.2m$) and B its beam ($B = 0.18m$). During the experiments, the draft is $D = 0.075m$. The maritime hull that has been analyzed is a classical Wigley hull noted WH2, where 2 remains the value of the exponent n in (3), of block coefficient $C_b = 0.67$. However, the block coefficients of river ships are around $0.80 - 0.90$. Then another Wigley-based hull of block coefficient $C_b = 0.89$, noted WH8 and for which $n = 8$ in (3), has also been analyzed. This results in a heavier hull shape at the bow and the stern of the ship (Figure 2).

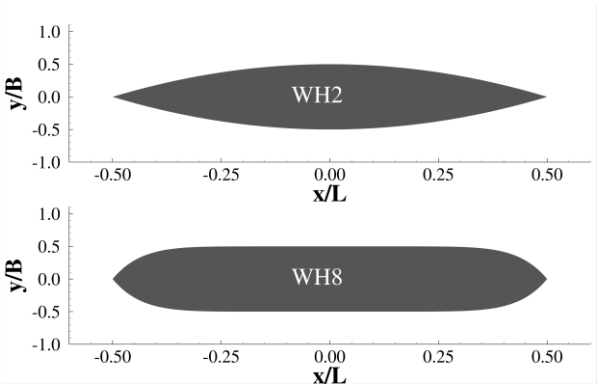

Fig. 2: Comparison of the shape of the WH2 maritime hull and the WH8 river hull.

1.2 *The towing tank and the waterway*

The wakes have been generated in the towing tank of the Institut Pprime. This canal is $20m$ long and has a rectangular section of width $W = 1.5m$. The water level can be set up to $1.2m$ and a double bottom can be placed in the canal, to reduce the water level while maintaining the ship hull and the measurement tools fixed (Figure 3). A carriage tows the ship hull along

the longitudinal axis of the canal at a speed up to $2.35m.s^{-1}$. During the trial, the hull is kept fixed with a vertical mast so that roll, pitch and yaw motions are impossible. Finally, the canal is equipped with windows on its left-side, which allows side-visualizations during the experiments.

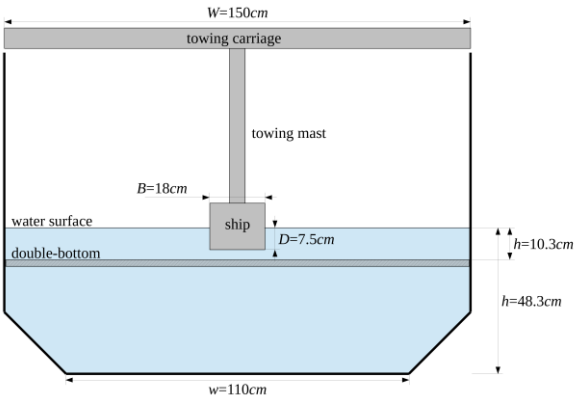

Fig. 3: Sketch of the transverse section of the towing tank and the ship hull. The towing tank has a trapezoidal transverse section in the deep water configuration ($h = 48.3cm$). A double bottom is placed to elevate the bottom of the canal and convert the transverse section to a rectangular one in the confined water configuration ($h = 10.3cm$).

The dimensional parameters for the deep water and confined water configurations have been established on the basis of two thresholds. First, a relation established by Zhu, *et al.*[27] gives a threshold on the height-based Froude number, from which the finite water depth has an effect on the undulatory behavior of the generated waves. From observations on analytically calculated shallow water ship wakes, the authors have assumed that for $F_h > 0.58$ the effects of finite water depth show up. Conversely, the water depth can be considered as infinite for height-based Froude numbers below this threshold. However, this threshold does not reflect the apparition of the hydrodynamic phenomena in the waterway. Thus, an empirical classification established by the International Towing Tank Conference[28] has been considered. This classification gives limit ratios between the geometric parameters of the waterway and the ship, which correspond to the apparition of the effects of the confinement of the waterway from a hydraulic point of view. These ratios are $h/D = 4$ for the vertical confinement, $W/B = 4$ for the lateral confinement, and $m = A_s/A_c = 0.0625$ for both.

Considering this, the wakes have been measured for two advancing speeds $U = 0.80m.s^{-1}$ and $U = 1.20m.s^{-1}$ and two water depths $h = 0.483m$ (deep water configuration) and $h = 0.103m$ (confined water configuration). This set of parameters, summarized in Table 1, allows to cover a wide range of height-based Froude numbers, while staying under the limit length-based Froude number $F_L = 0.50$ from which the angle starts to decrease[10-17]. In addition, the wide range of height-based Froude numbers allows to investigate subcritical, transcritical and supercritical wake shapes. As regards the hydraulic confinement, the width of the canal is the same for each configuration so the lateral confinement will be the same. However, the shallow water configuration is representative of the navigation in confined waters, as both undulatory ($F_h > 0.58$) and hydraulic ($h/D < 4$ and $m < 0.0625$) confinement are taken into account.

	Deep water		Confined water	
$h(m)$	0.483		0.103	
$U(m.s^{-1})$	0.80	1.20	0.80	1.20
F_L	0.23	0.35	0.23	0.35
F_h	0.37	0.55	0.80	1.20
$m = A_s/A_c$	0.088		0.019	
h/D	6.4		1.4	
W/B	8.3			

Table 1: Parameters of the experiments.

Finally, the ship resistance has been measured in the deep water configuration for a range of length-based Froude numbers F_L between 0.13 and 0.63, corresponding to height-based Froude numbers F_h between 0.20 and 1.00. As regards the shallow water configuration, the range of length-based Froude numbers is almost the same (between 0.18 and 0.54). However, as the water depth is smaller, the height-based Froude numbers range from 0.60 to 1.85. Hence, this allows to investigate the behavior of the ship resistance around the height-based Froude number $F_h = 1.00$. In addition, the chosen ship speeds cover the theoretical values of the critical height-based Froude numbers F_{h1} and F_{h2} calculated by the hydraulic Schijf's theory[21]. Figure 4 represents the values of F_{h1} and F_{h2} against the blockage ratio of the water way, and both studied configurations are reminded. In the case of the deep water configuration, the critical height-based Froude numbers corresponding to the blockage ratio $m = 1/53.7 = 0.019$ are $F_{h1} = 0.83$ and $F_{h2} = 1.17$. For the confined water configuration, the blockage ratio $m = 1/11.4 = 0.088$ gives the theoretical values $F_{h1} = 0.65$ and $F_{h2} = 1.37$.

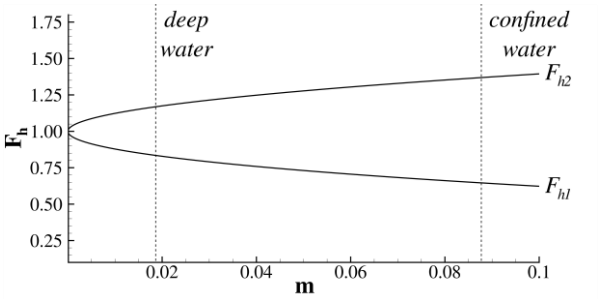

Fig. 4: The curve represents the theoretical values of the critical height-based Froude numbers F_{h1} and F_{h2} given by the hydraulic Schijf's theory[21] as a function of the blockage ratio m. The dotted lines emphasize the deep and confined water configurations of the experiments.

1.3 *Measurement tools*

1.3.1 *The stereo-correlation method*

The wakes have been measured with an optical measurement method based on a stereo-correlation principle[29]. The method consists in recording the deformation of the free surface during the passage of the ship with two cameras. The latter ones (Jai RM-4200CL that deliver a resolution of 2048×2048 pixels and equipped with Nikkor AF 28mm 1:2.8 lenses) are placed 1.5m above the surface of water. They focus on the same zone with an opposite angle of ±15° with respect to the longitudinal axis of the canal, and ±35° with respect to the vertical axis. The common field covered by the cameras forms a rectangle of dimensions $0.75 \times 0.90\, m^2$, corresponding to the half width of the canal. The acquisition of the images is performed with a R&D Vision system, composed by the Hiris software piloted by a synchronization box EG. Then the cameras are synchronized with the start of the ship and the exposure time is set to $10ms$. The frequency of the acquisition of the images is set at 10 frames per second (fps). The first step of the stereo-correlation method consists in the calibration of the cameras. For that, a two-dimensional target of points is displaced in the air, along the longitudinal axis of the canal and the camera models are calculated with a dedicated algorithm. Then the canal can be filled up and the surface of water is sowed with floating perlite particles, of size between $1 - 5mm$. These particles serve as markers that will follow the free surface deformations at the passage of the ship. Each run is performed three times to check the reproducibility of the measurement. Once the images have been recorded, a correlation algorithm based on the SLIP library[30] processes the image pairs. The free surface deformation is calculated at each time step with a spatial resolution of $10mm$ and a precision of the water level of $0.1mm$. Finally, from the three wave fields calculated at each time step, a mean wave field is calculated. Then, the whole wake is reconstructed around the ship hull with a dedicated reconstruction program. The result is shown in Figures 5 and 6, on which the black color represents the zones where the computing of the correlation is impossible because of either the absence of particles (chased away by the hull in the middle zone of the waterway), too high wave amplitudes on the banks or wave breaking.

1.3.2 *The multicomponent dynamometer and side-visualizations camera*

A multicomponent dynamometer Kistler 9272 is placed between the towing mast, which imposes the advancing speed, and the ship hull. It gives access to the three axial components of the force that opposes to the longitudinal motion of the hull, and the momentum around the vertical axis. As the hull is symmetrical and is aligned with the longitudinal axis of the canal, the transverse component of the force and the momentum around the vertical axis are negligible. Hence, only the longitudinal component of the ship resistance is considered for the calculation of the resistance coefficients. During the resistance trials, a high-speed camera has been placed on the side of the canal to access to a side-view of the wake generated by the ships, through the windows of the canal. A Photron Fastcam SA1.1 camera, which delivers a resolution of 1024×1024 pixels and equipped with a Sigma 28mm F1.8 DG Aspherical Macro lens, performs the acquisition of the images at a frequency of 125fps and is synchronized with the start of the ship. Then, the images are merged into one single image (Figure 8) with a dedicated C++ program based on the SLIP library[30].

2. Results

2.1 *Ship wakes*

The wakes measured in the deep water and confined water configurations are given in Figures 5 and 6, on which the non-dimensional water depth is given as a percentage of the initial water $h = 0.483m$ or $h = 0.103m$. The right part of each wake corresponds to the maritime hull WH2 and the left one corresponds to the river hull WH8. The wakes measured in the deep water configuration correspond to the classical Kelvin wake pattern, reflecting on the walls of the canal. Whatever the ship speed and its shape, the wake is composed of a transverse and a divergent wave system. A fast geometrical analysis leads to a value of the angle defining the envelop of the wake close to the Kelvin angle $\alpha = 19.47°$. There are no differences as regards the wavelengths of both wave systems, however, a small phase difference can be observed at the fastest ship speed (Figure 5b) between the wave systems generated by the two ship hulls. However, the higher block coefficient of the river hull generates a higher bow wave in both cases, and also non-linear components deforming the wake as well as higher wave amplitudes in the wave field. A focus on the walls of the canal, for a longitudinal position X/L between 0.5 and 2, highlights these differences. Indeed, for a length-based Froude number $F_L = 0.23$ (Figure 5a), the maximum peak-to-trough amplitudes on the wall correspond to 4% of the initial water depth for the maritime hull WH2 and 10% for the river hull WH8. That represents an increase of 150% of the amplitudes of the wash waves reflecting on the walls. For the length-based Froude number $F_L = 0.35$ (Figure 5b), the difference is less important as the peak-to-trough amplitudes are respectively of 11% and 15% of the initial water depth for the maritime and river hulls, representing an increase of 40% of the wave amplitude. In both cases, the waves generated by the river hull are more destructive. Finally, there are no visible effects of the vertical confinement, on both wake shape and angle,

however the lateral confinement implies multiple wave reflections on the walls. Hence, the bow and stern wakes interact and superimpose, leading to the apparition of caustics in the wakes.

As regards the wakes generated in the confined water configuration (Figure 6), the effects of both lateral and vertical confinement are present. First, for the length-based Froude number $F_L = 0.23$, corresponding to a height-based Froude number $F_h = 0.80$, the wake is transcritical from a undulatory point of view: the transverse waves have disappeared and the wake is composed only of divergent waves. As regards the hydraulic confinement, two phenomena highlighted by Scott Russell[18] have appeared around the ships. The bow wave has straightened up and is perpendicular to the ship, and the lowering of the water level around the hulls extends up to the walls of the canal. In addition, there is a wave-breaking of the first transverse wave generated by the river hull WH2, which represents a risk for the river banks. For the length-based Froude number $F_L = 0.35$, corresponding to a height-based Froude number $F_h = 1.20$, the wake is supercritical. The wake is now composed only of divergent waves and the bow wave starts to fold backwards to the ship[3,8]. This behavior is reminiscent of the Mach cone in supersonic aerodynamics.

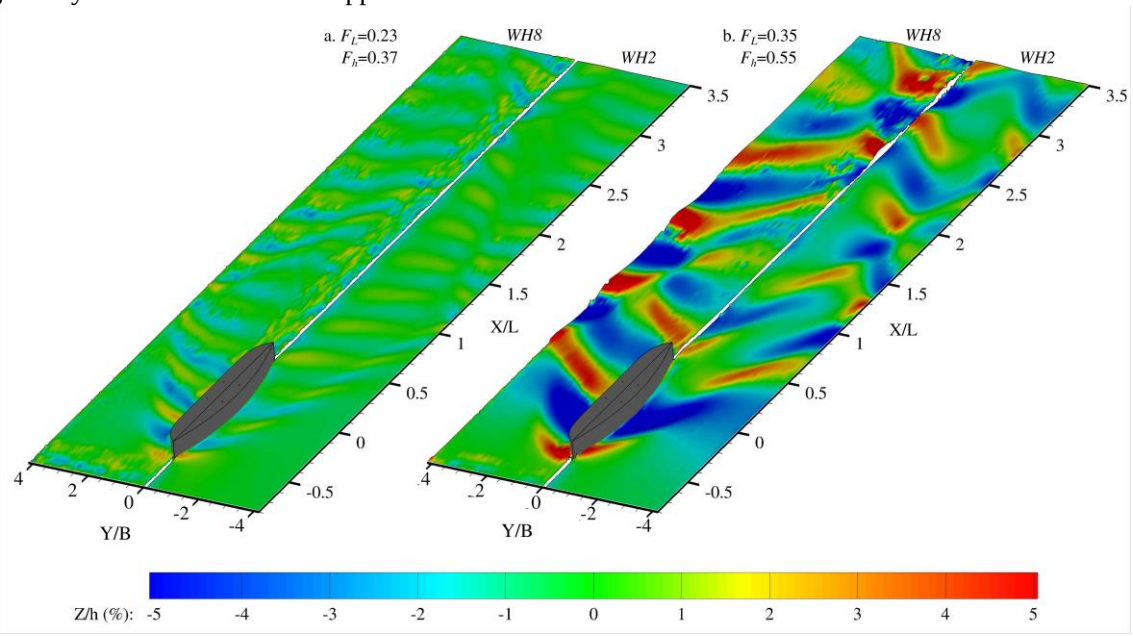

Fig. 5: Ship wakes measured in the deep water configuration. Left (a): F_L=0.23, F_h=0.37 – Right (b): F_L=0.35, F_h=0.55. The right part of each wake corresponds to the maritime hull WH2 and the left one corresponds to the river hull WH8.

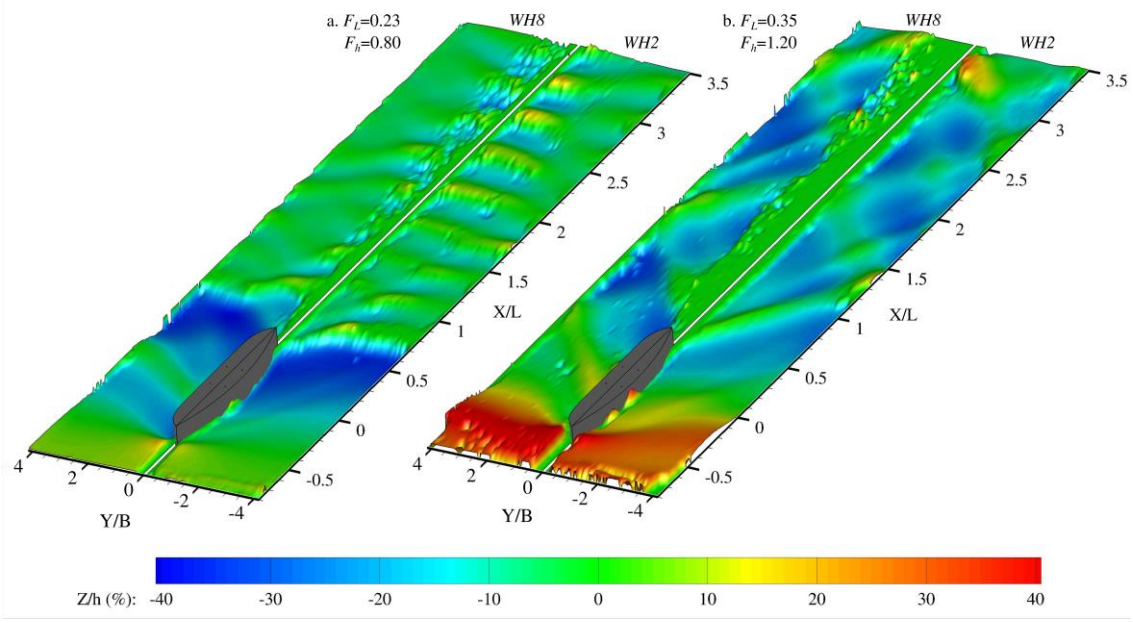

Fig. 6: Ship wakes measured in the confined water configuration. Left (a): F_L=0.23, F_h=0.80 – Right (b): F_L=0.35, F_h=1.20. The right part of each wake corresponds to the maritime hull WH2 and the left one corresponds to the river hull WH8.

2.2 *Resistance curves*

Figure 7 represents the resistance coefficients C_d of the ship hulls as a function of both length-based and height-based Froude numbers F_L and F_h (respectively the bottom and top x-axes), for the deep water configuration (left) and the confined water configuration (right). The dotted black lines correspond to the ship speeds for which the wakes have been measured, and the dashed black lines correspond to the theoretical values of the critical height-based Froude numbers given by Schijf's theory[21]. The error bars represent the dimensionless measurement uncertainty of the resistance coefficient, derived from the measurement uncertainty of the drag force calculated with the GUM method[31,32]. The resistance coefficient C_d gives a non-dimensional vision of the ship resistance with the ship speed. It is calculated with the formula (4), in which $R(N)$ is the measured force, $\rho = 1000\ kg/m^3$ the density of the water in the canal and $U(m.s^{-1})$ the ship speed. The quantity $S(m^2)$ corresponds to the wetted surface area of the ship, calculated with (5), in which $\delta(x)$ defines the contour of the wetted cross-section of the ship hull[33]. After calculation, the equation (6) is found, giving the relation between the wetted surface area and the geometric parameters of the hulls. In the case of the studied hulls, $S_{WH2} = 0.324m^2$ and $S_{WH8} = 0.372m^2$.

$$C_d = 2R/\rho SU^2 \quad (4)$$

$$S=\int \delta(x)dx=2\int [y(x)+D]dx \quad (5)$$

$$S=L[2D+BC_b] \quad (6)$$

For the deep water configuration, there are oscillations in the resistance of the ship for length-based Froude numbers $F_L < 0.35$, especially for the maritime hull WH2. These oscillations correspond to the interaction between the bow and stern waves whose wavelengths depend on the speed of the ship. So depending on the ship speed, the constructive or destructive interferences of these two wave systems will generate oscillations in the ship resistance. In addition, for a length-based Froude number $F_L > 0.45$, the resistance coefficient is constant and starts to decrease for a ship speed corresponding to a height-based Froude number $F_h > F_{h1} > 0.83$. Finally, the higher block coefficient of the river hull WH8 implies a higher resistance coefficient, as the displaced volume of water is more important. The resistance coefficients measured in the confined water configuration have a different behavior with the ship speed and are quantitatively higher than in deep water. The theoretical values of the critical height-based Froude numbers F_{h1} and F_{h2} given by Schijf's theory[21] correspond to drastic changes in the resistance coefficient value. First, there is a sharp increase of the resistance coefficient value for a height-based Froude number $F_h > F_{h1} > 0.65$. This sharp increase is followed by a plateau on which the resistance coefficient is constant and then the resistance coefficient decreases suddenly for a height-based Froude number $F_h > F_{h2} > 1.37$. The visualizations given in Figure 8 highlight the causes of the variations of the resistance coefficient. First, the sharp increase corresponds to the moment when the transverse waves are stuck at the stern of the ship. Then during the plateau, the bow wave appears and its amplitude slowly increases. The sudden decrease of the resistance coefficient corresponds to the moment when the ship passes over its own bow wave and rides it.

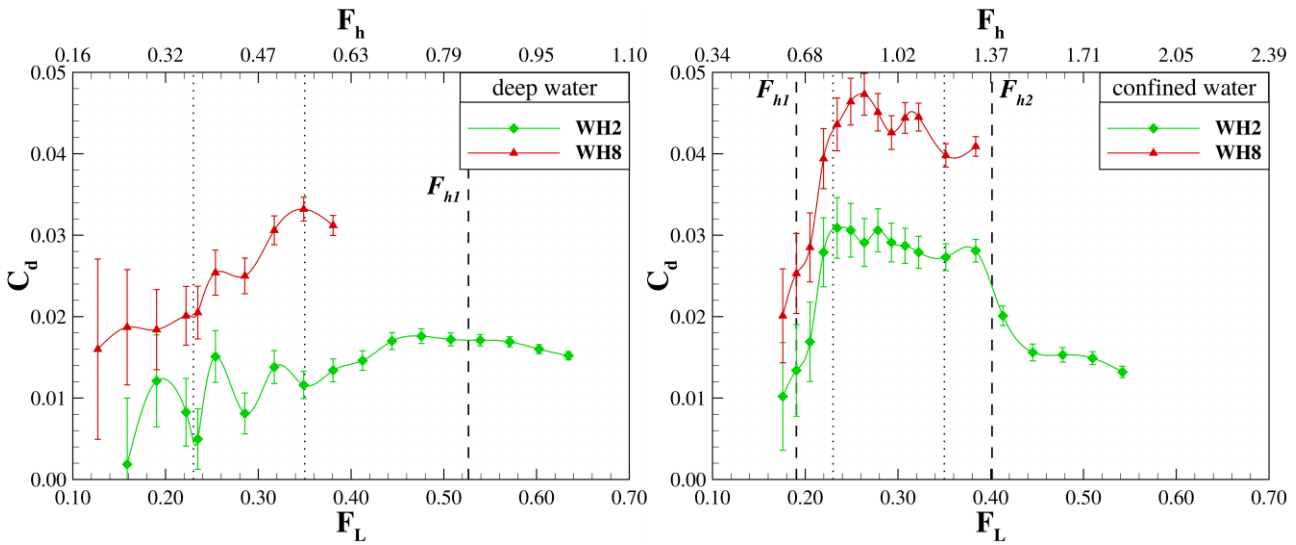

Fig. 7: Resistance coefficients C_d of the ship hulls as a function of the length-based (bottom x-axis) and height-based (top x-axis) Froude numbers F_L and F_h. The dotted black lines remind the ship speeds for which the wakes have been measured with the stereo-correlation method. The dashed black lines correspond to the theoretical values of the critical height-based Froude numbers F_{h1} and F_{h2}. Left: deep water configuration – Right: confined water configuration.

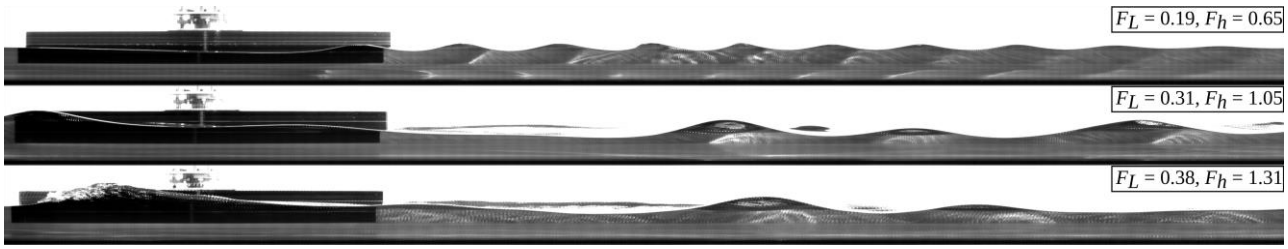

Fig. 8: Side view of the wakes generated by the maritime hull WH2 in the confined water configuration during the resistance trials, for three different ship speeds (going right to left). Top: F_L =0.19, F_h=0.65 – Middle: F_L =0.31, F_h=1.05 – Bottom: F_L =0.38, F_h=1.31.

2.3 *Influence of the trim on the ship resistance*

Experiments have been carried out to identify the influence of the trim of the ship on its resistance coefficient in the different regimes. For that, the fixed-hull setup has been modified into a free-hull setup with the adaptation of a hinge system between the hull and the hydrodynamic balance, allowing it to trim. The ship resistance has been measured for the WH8 river hull in a shallow water configuration of trapezoidal cross-section with the following parameters: $h = 0.103m$, $W = 1.30m$, $w = 1.10m$ and $D = 0.04m$. These waterway parameters give a blockage ratio $m = 1/17.2 = 0.058$ corresponding to critical height-based Froude numbers $F_{h1} = 0.71$ and $F_{h2} = 1.30$. The resistance force measurements have been made with the fixed-hull system and the free-hull system and the results are given in Figure 9, on which the error bars represent the dimensionless measurement uncertainty.

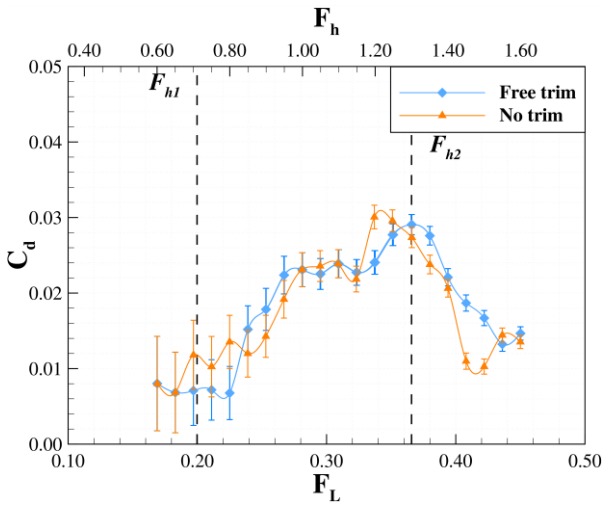

Fig. 9: Resistance coefficients C_d of the ship hull WH8 in confined water as a function of the length-based (bottom x-axis) and height-based (top x-axis) Froude numbers F_L and F_h. The dashed black lines correspond to the theoretical values of the critical height-based Froude numbers F_{h1} and F_{h2}. Blue (squares): free trim configuration – Orange (triangles): fixed-hull configuration. The error bars represent the estimated measurement uncertainty of the resistance coefficient.

These results show that the trim of the ship seems to have an influence in the transition between the sub- and transcritical regimes (*i.e.* around the critical height-based Froude number $F_{h1} = 0.71$), although in the transcritical regime the resistance coefficient is the same with or without trim. In the supercritical regime the trim has a strong effect and shifts the peak of maximum resistance. The visualizations made during these experiments show that the stern sinkage increases with the ship speed and the apparition of the bow wave. The trim angle is maximum at the critical height-based Froude number $F_{h2} = 1.30$, where the resistance is at its maximum as well as the bow wave amplitude. The surfing of the bow wave still occurs above that ship speed, but the trim increases the wetted surface of the hull and so the ship resistance.

3. Conclusions

The wakes generated by hulls representative of maritime and river ships have been measured in a towing tank. The non-intrusive optical measurement method allowed to identify various wake shapes generated in deep water and confined water configurations, for different ship speeds. The results highlighted the effects of both ship and waterway geometries on the generated wakes. In the deep water configuration, the influence of the ship block coefficient on the amplitude of the wash waves has been characterized. In the confined water configuration, transcritical and supercritical wakes have been identified and compared. The effects of the vertical and lateral confinement on both undulatory and hydraulic components of the wakes have been studied. Their influence on the resistance of the ship has been emphasized during the resistance trials, combined with side-visualizations of the wakes. The influence of the trim of the ship hull on its resistance coefficient in the sub- and supercritical regimes has also been highlighted. However, in a real canal configuration, the current has a strong influence on these parameters. Hence, the measurement of both ship wakes and resistance in a presence of a co- and counter-current of river are necessary. This is our current line of research...

4. Compliance with ethical standards

Conflict of Interest: The authors declare that they have no conflict of interest.

Funding: There is no funding source.

Ethical approval: This article does not contain any studies with human participants or animals performed by any of the authors.

5. References

[1] Ekman V.W. On stationary waves in running water [J]. *Arkiv för matematik, astronomi och fys*ik, 1906, 3(2).

[2] Ekman V.W. On the waves produced by a given distribution of pressure which travels over the surface of water [J]. *Arkiv för matematik, astronomi och fys*ik, 1907, 3(11).

[3] Havelock T.H. The propagation of groups of waves in dispersive media, with application to waves on water produced by a travelling disturbance [J]. *Proceedings of the Royal Society A: Mathematical, Physical and Engineering Sciences*, 1908, 81(549):398-430.

[4] Inui T. (Teturô). On deformation, wave patterns and resonance phenomenon of water surface due to a moving disturbance [J]. *Proceedings of the Physico-Mathematical Society of Japan, 3rd Series*, 1936, 18:60-98.

[5] Crapper G.D. Surface waves generated by a travelling pressure point [J]. *Proceedings of the Royal Society A: Mathematical, Physical and Engineering Sciences*, 1964, 282(1391):547-558.

[6] Fang M.C., Yang R.Y., Shugan I.V. Kelvin ship wake in the wind waves field and on the finite sea depth [J]. *Journal of Fluid Mechanics*, 2011, 27(01):71-77.

[7] Carusotto I., Rousseaux G. The Čerenkov effect revisited: from swimming ducks to zero modes in gravitational analogues [J]. *Analogue Gravity Phenomenology*, 2013, 6:109-144.

[8] Elsaesser B. The characteristics, propagation and transformation of waves generated by fast marine crafts [D]. Belfast, Northern Ireland: Queen's University of Belfast, 2004.

[9] Kelvin W.T. On ship waves [J]. *Proceedings of the Institutions of Mechanical Eng*ineers, 1887, 38(1):409.

[10] Taylor D.W. Resistance of ships and screw propulsion [M]. New-York, U.S.A.: Macmillan and Co, 1893.

[11] Hovgaard W. Diverging Waves [J]. *Transactions of the Royal Institution of Naval Architects, London*, 1909, 51:251-261.

[12] Baker G. Ship form, resistance and screw propulsion [M]. London, England: D. Van Nostrand Company, 1915.

[13] Whitham G. B. Linear and nonlinear waves [M]. New-York, U.S.A.: John Wiley & Sons, 1974.

[14] Rabaud M., Moisy F. Ship wakes: Kelvin or Mach angle ? [J]. *Physical Review Letters*, 2013, 110(21):214.

[15] Noblesse F., He J., Zhu Y., Hong L., Zhang C., Zhu R., Yang C. Why can ship wakes appear narrower than Kelvin's angle ? [J]. *European Journal of Mechanics – B/Fluids*, 2014, 46(0):164-171.

[16] Darmon A., Benzaquen M., Raphaël E. Kelvin wake pattern at large Froude numbers [J]. *Journal of Fluid Mechanics*, 2014, 738, R3.

[17] Pethiyagoda R., McCue S.W., Moroney T.J. What is the apparent angle of a Kelvin ship wave pattern ? *[J]. Journal of Fluid Mechanics, 2014, 758:468-485*.

[18] Scott Russell J. Experimental researches into the laws of certain hydrodynamical phenomena that accompany the motion of floating bodies have not previously been reduced into conformity with known laws of the resistance of fluids *[J]. Transactions of the Edinburgh Royal Society*, 1840, 14:47-109.

[19] Inui T. (Takao). Wave-making resistance in shallow water sea and in restricted water with special reference to its discontinuities [J]. *The Japan Society of Naval Architects and Ocean Engineers*, 1954, 76:1-10.

[20] Inui T. (Takao), Kikuchi Y., Iwata T. Shallow water effects on wave-making of ships - A comparison of calculated and measured resistance [J]. *Journal of Zosen Kiokai*, 1956, 100:35-45.

[21] Schijf J.B. (1949). – Protection of embankments and bed in inland and maritime waters, and in overflow or weirs [C]. *17th International Navigation Congress, Lisbon*, Portugal, 1949.

[22] Linde F., Ouahsine A., Huybrechts N., Sergent P.. (2017). – Three-dimensional numerical simulation of ship resistance in restricted waterways: effect of ship sinkage and channel restriction [J]. *Journal of Waterway, Port, Coastal and Ocean Engineering*, 2017, 43(1):06016003.

[23] Pacuraru F. and Domnisoru L. Numerical investigation of shallow water effect on a barge ship resistance [J]. *IOP Conference Series: Materials Science and Engineering*, 2017, 227 012088.

[24] Terziev M., Tezdogan T., Oguz E., Gourlay T., Demirel Y.K., Incecik A. Numerical investigation of the behaviour and performance of ships advancing through restricted shallow waters [J]. *Journal of Fluids and Structures*, 2018, 46:185-215.

[25] Caplier C., Rousseaux G., Calluaud D., David L. Energy distribution in shallow water ship wakes from a spectral analysis of the wave field [J]. *Physics of Fluids*, 2016, 28(10):107104.

[26] Wigley W.C.S. Ship wave resistance. A comparison of mathematical theory with experimental results [J]. *Transactions of the Royal Institution of Naval Arch*itects, 1926, 14:124-141.

[27] Zhu Y., He J., Zhang C., Wu H., Wan D., Zhu R., Noblesse F. Far-field waves created by a monohull ship in shallow water [J]. *European Journal of Mechanics – B/Fluids*, 2015, 49(0):226-234.

[28] International Towing Tank Conference. Report of the Resistance and Flow Committee [C].

18th International Towing Tank Conference, Kobe, Japan, 1987.

[29] Chatellier L., Jarny S., Gibouin F., David L. A parametric PIV/DIC method for the measurement of free surface flows [J]. *Experiments in Fluids*, 2013, 54(3):1-15.

[30] Tremblais B., David L. Arrivault D., Dombre J., Thomas L., Chatellier L. Standard Library for Image Processing, (Licence CECILL DL 03685-01, APPIDDN.FR.001.300034.000.S.P.2010.000.21000) http://sliplib.prd.fr/, 2010.

[31] GUM: Guide to the expression of the Uncertainty in Measurement. *Working Group 1 of the Joint Committee for Guides in Metrology (JCGM/WG 1)*, 1995.

[32] Caplier C. Etude expérimentale des effets de hauteur d'eau finie, de confinement latéral et de courant sur les sillages et la résistance à l'avancement des navires [D]. Poitiers, France: University of Poitiers, 2015.

[33] Bindel S. Hydrodynamique Navale. I, généralités, résistance. [M]. Paris, France: Les Presses de l'E.N.S.T.A., 1972.